Coherent Longitudinal Acoustic Phonons in Three-Dimensional Supracrystals of Cobalt Nanocrystals

Isabelle Lisiecki, Dario Polli, Cong Yan, Giancarlo Soavi, Eugène Duval, Giulio Cerullo, Marie-Paule Pileni

DOI: 10.1021/nl4028704

Coherent Longitudinal Acoustic Phonons in Three-Dimensional Supracrystals of Cobalt Nanocrystals

Isabelle Lisiecki,[†,‡] Dario Polli,[§] Cong Yan,[†,‡] Giancarlo Soavi,[§] Eugène Duval[∫], Giulio Cerullo[§] and Marie-Paule Pileni[†,‡,]*

[†] Université Pierre et Marie Curie, UMR 7070, LM2N, 4 place Jussieu 75005 Paris, France

[‡] Centre National de la Recherche Scientifique, UMR 7070, LM2N, 4 place Jussieu 75005 Paris, France

[§] IFN-CNR, Dipartimento di Fisica, Politecnico di Milano, P.za L. da Vinci 32, 20133 Milano, Italy

[∫] Université Lyon 1, Institut Lumière Matière, CNRS, UMR 5586, F-69622 Villeurbanne Cedex, France

KEYWORDS: nanocrystals, fcc supracrystals, picosecond acoustics, time-resolved spectroscopy, longitudinal acoustic phonons.

ABSTRACT We use broadband picosecond acoustics to detect longitudinal acoustic phonons with few-GHz frequency in three-dimensional supracrystals (with face-center cubic lattice) of 7-nm cobalt nanocrystal spheres. In full analogy with atomic crystals, where longitudinal acoustic phonons propagate with the speed of sound through coherent movements of atoms of the lattice out of their equilibrium positions, in these supracrystals atoms are replaced by (uncompressible) nanocrystals and atomic bonds by coating agents (carbon chains) which act like mechanical springs holding together the nanocrystals. Repeating the measurements at different laser angles of incidence it was possible to accurately determine both the index of refraction of the supracrystal ($n=1.26\pm0.03$) and the room-temperature longitudinal speed of sound ($v_s= 1235\pm12$ m/s), which is quite low due to the heavy weight of the spheres (with respect to atoms in a crystal) and the soft carbon chains (with respect to atomic bonds). Interestingly, the speed of sound inside the supracrystal was found to dramatically increase by decreasing the sample temperature, due to a change in the stiffness of the dodecanoic acid chains which coat the Co nanocrystals.

TEXT

Artificial colloidal crystals of spherical metallic nanocrystals (NCs) with mesoscopic dimensions are extensively studied [1-15] and show collective physical (magnetic, mechanical etc…) properties due to the nanocrystal ordering [16-27]. Inorganic NCs can self-organize into ordered three-dimensional (3D) structures with a face-centered cubic (fcc) Bravais lattice called supracrystals [1, 28]. The physical properties of these supracrystals are quite different from those of disordered aggregates as well as both isolated NCs and the bulk phase [21]. Here we investigate another analogy between the usual crystals made of atoms and the supracrystals made of NCs: coherent longitudinal acoustic (LA) phonon propagation (Fig. 1(a)). In usual crystals, LA phonons (also termed compression waves) are coherent movements of atoms of the lattice out of their equilibrium positions in the direction of propagation with sound speed v_s, which is a function of the Young's modulus, the Poisson's modulus and the density of the material. In supracrystals we can draw a full analogy with atomic crystals, where atoms are replaced by (uncompressible) NCs and atomic bonds by coating agents (carbon chains) which act like mechanical springs holding together the NCs. We report here on the impulsive excitation and broadband detection of LA phonons in cobalt supracrystals, traveling at significantly lower speed with respect to their analogs in atomic crystals, due to the large particle mass and the loose interparticle bonds.

The sample is a compact self-organized 3D fcc supracrystal (Fig. 1(b)) consisting of polycrystalline Co NCs with 7.1-nm mean diameter and 9.5% size distribution [29], held together by dodecanoic acid chains which coat the NCs and act like stiff mechanical springs and prevent coalescence. The supracrystals are deposited on either highly ordered pyrolytic graphite (HOPG) [8] or silicon wafers. From grazing incidence small-angle X-ray scattering (GISAXS)

measurements, the center-to-center NC distance is found to be 10.1 nm, so that the average NC spacing is 3 nm. The supracrystal thickness varies from a few tens of nanometers to few micrometers [30]. See Supporting Information for details on sample preparation and characterization.

Analogously to conventional crystals, we excited and detected LA phonon waves in the supracrystals using the picosecond acoustics (PA) technique. PA is a powerful time-domain optical method that enables the generation and detection of ultrasounds up to several hundred GHz frequency range [31, 32]. It has been intensively used for probing elastic properties of thin films and multilayers and consists in a pump-probe experiment in reflection geometry. A first pump pulse at 800 nm (with 150-fs duration, ≈1-μJ energy and 1-kHz repetition rate, delivered by a commercial regeneratively amplified Ti:Sapphire laser) is focused on the sample (see Fig. 1(a)) and absorbed by the transducer (HOPG or Silicon substrate). This induces an "instantaneous" thermal expansion which impulsively creates a travelling compression wave (i.e. a phonon wavepacket with broad spectrum) which moves in the sample with the longitudinal speed of sound v_s. Such localized strain wave results in a moving discontinuity in the material index of refraction, corresponding to a mirror able to partially reflect a second delayed probe pulse with broadband spectrum in the visible (covering the 460-720 nm wavelength range) through a stimulated Brillouin scattering (SBS) process. SBS can be explained either from a quantum point of view imposing energy and momentum conservation for the photon/phonon scattering event or using a classical wave description considering two simultaneous effects: (i) Bragg law for reflection (i.e. constructive interferences arising when the wavelength of light is a multiple of the acoustic wavelength) and (ii) Doppler shift (the frequency of the reflected light is shifted by the moving acoustic wave). The probe light reflected at the moving discontinuity

interferes with that reflected at the (fixed) substrate, thus creating periodic constructive/destructive modulations in the two-dimensional (2D) transient reflectivity maps measured using a single-shot spectrometer [33]. The signal is calculated as $\Delta R/R(\lambda_{pr},\tau)= (R^{on}-R^{off})/R^{off}$, where R^{on} and R^{off} are the reflected probe intensities with and without the pump pulses, λ_{pr} and τ are the probe wavelength and delay. From a simple calculation of the intensity resulting from the interference, the period T of the $\Delta R/R$ oscillation is thus proportional to the probe wavelength λ_{pr} through the formula:

$$T = \frac{\lambda_{pr}}{2v_s \cdot n \cdot \cos\vartheta'} = \frac{\lambda_{pr}}{2v_s \cdot \sqrt{(n^2 - \sin^2\vartheta)}} \quad (1)$$

where n is the sample refractive index, ϑ' is the angle between the photon and phonon wavevectors inside the sample and ϑ is the (external) angle of incidence of the probe light (see Fig. 1(a)).

Figures 2(a) and 2(c) show the 2D $\Delta R/R$ maps for Co supracrystal samples deposited on either HOPG (a) or a silicon wafer (c) at quasi-normal angle of incidence ($\vartheta_1 = 6°$). Oscillations of the $\Delta R/R$ signal are clearly observed, with variable periodicity depending on the probe wavelength. To better highlight this effect, in all the four panels of Figure 2 we plotted the isolated oscillating components obtained by subtracting the slowly varying background signal. Dynamics at selected λ_{pr} were extracted from the 2D maps by horizontal cuts of Fig. 2(a,c) and displayed in Fig. 2(b,d) for HOPG and silicon substrates, respectively. It is evident that the oscillation dynamics for HOPG and silicon substrates are perfectly superimposed, demonstrating that they do not depend on the material used as transducer for inducing the travelling acoustic wave inside the supracrystal. We also performed several control measurements on a bare HOPG substrate (not shown here) and we could not detect any oscillation, indicating that they do not originate from

travelling acoustic waves inside the substrate (which would anyway display tens of times higher frequency and travel at considerably higher speed).

We also note that the oscillation pattern is anharmonic: the observed frequency slightly reduces as a function of time for any given probe wavelength (see Fig. 2(b,d)). This feature is not found to depend on the pump pulse energy and could be explained by two different mechanisms: (i) *a thermalization process*: an increase of temperature of the dodecanoic network after the transfer of vibrational energy (not yet heat) from Co NCs to the dodecanoic supracrystalline film; (ii) *variable density of the sample*: for increasing time delays following the LA phonon excitation by the pump pulse, the acoustic wavepacket propagates from the substrate towards the surface. The sample density could accordingly reduce, thus causing a moderate reduction of the speed of sound.

In Fig. 3(a) we plot the extracted period of the oscillations T as a function of λ_{pr}, obtained by evaluating the inverse of the frequency peak of the Fourier transform of the dynamics in Fig. 2. The results are nearly identical for HOPG (blue diamonds) and silicon (black circles) substrates and they present a perfectly linear dependence as expected from Eq. (1). From linear fits $T = \beta\lambda_{pr}$ we could extract the proportionality constants of β_1=309fs/nm (HOPG, dashed blue line) and 306fs/nm (silicon, solid black line). Note that the fit has been performed with zero intercept, because the dispersion relationship between frequency ω and phonon wavevector k is linear at such low-frequency phonons, resulting in a constant sound speed $v_S = \frac{\partial\omega}{\partial k} \cong \frac{\omega}{k}$ (i.e. phase and group velocities are equal). We note that similar low-frequency (few GHz) oscillations were recently observed in samples of silica nanoparticles held together either by van der Waals or covalent interactions [34], but were interpreted in terms of standing acoustic waves of a ≈200-nm slab of material impulsively excited by the ultrashort pump pulse.

From Eq. (1) the proportionality constant $\beta = \left\{2v_s \cdot \sqrt{(n^2 - \sin^2\vartheta)}\right\}^{-1}$ contains three parameters: the external incidence angle (measured), the index of refraction n and the speed of sound v_s. A set of two measurements of β for two different angles ϑ should then be sufficient to simultaneously determine both n and v_s. To improve the accuracy in the extracted values, we decided to perform measurements at three different angles (on HOPG substrate). Figure 3(a) reports the results for ϑ_2=62° (red squares) and ϑ_3=80° (green triangles). Similarly to the previous case (ϑ_1=6°), we observe a linear dependence of the extracted oscillating period T on the probe wavelength λ_{pr}, with a proportionality constant which increases for increasing angle as expected from Eq. 1: β_2=440 fs/nm at ϑ_2=62° and β_3=488 fs/nm at ϑ_3=80°. $\Delta R/R$ time traces at λ_{pr}= 550 nm for the three angles of incidence on the same sample position are plotted in Fig. 3(b) to better visualize the increase of T with ϑ. Putting together the three measurements we could estimate the index of refraction n = 1.26±0.03 and the speed of sound v_s = 1235±12 m/s. This low value for the speed of sound can be explained considering the large mass of the NCs and the rather weak interactions between the interdigitized dodecanoic chains.

Let us now discuss the role of the thickness of the sample related to the sound attenuation, the penetration depth of the laser and the index of refraction of the structure. In the best conditions we could detect LA phonon propagation up to a maximum delay of T_{max}≈800 ps. Considering the extracted speed of sound, this corresponds to a maximum distance of propagation of v_s * T_{max} ≅ 1 μm. Fitting the oscillations with a damped sinusoidal curve we could extract an average damping time of τ≅210 ps. Such a fast damping could be associated to the interplay of two main phenomena. First, sound attenuation due to absorption and/or scattering of the LA phonons during propagation must be taken into account. If this were the only responsible for the extracted dynamics, the mean free path for phonons would be l=2*v_s*τ ≅ 520 nm [35], corresponding to a

sound attenuation of $\Gamma = \frac{v_s}{2\pi l} \cong 380$ MHz. A second contribution comes from the relatively small thickness of the supracrystal. The sample in fact does not possess a homogeneous thickness under the probed area (≈50x50μm in the case of normal incidence): some areas are very thin (tens of nanometers), some others could be in excess of 1 μm, so that for longer time delays only the few relatively thick areas contribute to the signal. Let us now verify that the pump/probe pulses can indeed travel within ≈1 μm thickness supracrystal. For this purpose we employ a simple effective medium theory such as the Maxwell-Garnett mixing rule [36], which computes the dielectric properties of a multiphase mixture. We considered the complex permittivity of the cobalt spherical enclosures (with 7.1-nm diameter) and their ≈25.7% filling factor in the matrix (since the center-to-center NC distance is 10.1 nm and the lattice has fcc packing). We could then estimate the complex permittivity of the supracrystal (see Supporting Information), which results in an effective absorption coefficient in the range from $\alpha = 2.47$ μm^{-1} at the bluest probe wavelength 460nm (i.e. 10% transmission within 1μm) to $\alpha = 0.663$ μm^{-1} at 780-nm pump wavelength (i.e. 51% transmission within 1μm). This confirms that the pump pulse can indeed reach the substrate and efficiently excite it, launching the acoustic wave in the supracrystal, and that the probe light can penetrate the sample and detect the LA phonons. The Maxwell-Garnett mixing rule provides at the same time the (real) effective index of refraction of the supracrystal, which is calculated to be $n \cong 1.44$ at λ=600 nm, with ±0.02 variation due to dispersion in the visible wavelength range (see Supporting Information). This value is quite close to the experimental one, and the dispersion of the refractive index is very small, thus confirming the validity of the linear fit in Fig. 3(a). The ≈12% discrepancy in the index of refraction is probably due to two factors: (i) the Maxwell-Garnett mixing rule was derived under the assumption that the separation of the particles is sufficiently large to ensure independent scattering, so that it is

valid only for small enclosures (filling factors up to 20-30%); (ii) it does not take into account the size dispersion (9.5% in our case) of the NCs around the mean diameter. More sophisticated techniques could be applied but this is out of the scope of the paper.

We performed another set of measurements at variable sample temperature, in order to characterize the dependence of the speed of sound on temperature and highlight the role of the coating agents as springs connecting the NCs. We inserted the sample into a cryostat equipped both with a heater and a liquid nitrogen reservoir. Figure 4(a) shows $\Delta R/R$ dynamics at λ_{pr}=600 nm recorded at 110K, 295K and 435 K temperatures for the supracrystals on HOPG substrate at quasi-normal incidence. We observe a drastic dependence of the oscillation period on the temperature. From 435K to 110K the whole pattern of oscillations shrinks by nearly a factor of 5, i.e. almost proportionally to the temperature. This change in period is fully reversible, as verified by successively operating several cycles and observing no permanent modification of the sample. Following Eq. (1), the change of period with temperature can be ascribed only to a change of speed of sound or index of refraction, as for quasi-normal incidence the internal angle ϑ' can be considered constant ($\cos\vartheta' \cong \cos\vartheta \cong 1$). In Fig. 4(b) we plot the extracted values of the product $v_s \cdot n = \frac{1}{2\beta}$ obtained for a large set of measurements in the aforementioned temperature range. Unfortunately we cannot directly access the index of refraction as a function of temperature -as we did at room temperature- because our cryostat only works at quasi-normal incidence. Nonetheless, we argue that it cannot vary much in this temperature range and for sure it cannot be the only responsible for the observed effect (it would become lower than 1 at 435K). On the other hand, if the index of refraction were constant throughout the measurement range, the speed of sound would vary from ≈870 m/s at 435K to more than 3500 m/s at 110K (see the right axis in Fig. 4(b)). Note that this strong variation is at odds with the behavior of acoustic waves in

ordinary crystals, for which the speed of sound displays only a weak temperature dependence. A clear change of behavior is seen around 250K and two linear fits with different slopes and intercepts (as indicated in Fig. 4(b)) can describe the data. This is a very peculiar effect of this supracrystalline material, which has never been observed in normal crystals, where both the speed of sound and the index of refraction are almost insensitive of temperature. This temperature dependence of sound velocity is reminiscent of that observed in glass-forming materials in the supercooled state between the crystalline melting (T_f) and glass transition (T_g) temperatures [37]. As an example, in the glassy state of polycarbonate at 413 K (i.e. slightly below T_g=420 K), the longitudinal acoustic velocity is v_s=2130 m/s; on the other hand, at 513 K (i.e. slightly above T_f=523 K), v_s=1600 m/s [37].

From the qualitative behavior of v_s and n relatively to the density, it is deduced that the increase of v_s*n at low temperature in our sample is mainly due to an increase of the rigidity of the dodecanoic network: the lower the temperature, the higher their stiffness that in turn gives rise to an increase of the speed of sound. The crossing point at 250K can be assigned to a temperature transition, attributed to a phase transition of the alkyl chain configuration from ordered to disordered [38]. Depending on temperature, two different structural dynamics regimes can be established, corresponding to two different regimes of the rigidity of the bonds between the interdigitized alkyl chains. Molecular dynamics simulations of a similar system (dodecanethiol self-assembled monolayers on gold nanocrystals) [39] showed that at low temperatures (up to 200K) the passivating molecules organize into oriented molecular bundles with ordered parallel alignment. For higher temperatures intramolecular conformational defects (e.g. reduction of both the percentage of molecules with *trans* configuration and of their end-to-end length) induce disorder in the coating agents, which starts at the bundles' outer boundaries

and then with increasing temperature propagates inward towards the nanoparticle surface. At ≈290K melting of the molecular bundles occurs, resulting in a uniform (random) orientation of the molecules around the nanocrystals. Alkyl-chain dynamics were studied in a similar system [40] and were found to evolve continuously with increase in temperature: at low temperature only a small portion of each chain is dynamically active and only at 400 K the whole chain is involved. We note that a second phase transition of the alkyl chains from the *trans* configuration to a liquid-like phase takes place at 340K. No such transition is observed in our data, probably because it has no effect on the rigidity.

In conclusion, we successfully observed longitudinal acoustic wavepackets propagation in a self-assembled supracrystal film made of highly ordered NCs linked by alkyl chains, in analogy with atomic crystals. These waves are detected in the time domain using the broadband PA technique. Due to the large mass of the NCs and the low stiffness of the connecting alkyl chains, the oscillation period turns out to be quite long, of the order of 200 ps at room temperature. In contrast with ordinary solids, the speed of sound in these artificial materials is strongly dependent on temperature, due to the change in the dynamic properties of the dodecanoic lattices. To further explore such specific behavior of supracrystalline materials, similar experiments could be performed with smaller Co nanocrystals self-ordered in fcc supracrystals. We could expect to observe a change of the speed of sound by tuning the size of the nanocrystals and/or increasing the elastic modulus of the linking molecules until it becomes comparable to that of the nanocrystals themselves. Furthermore, we could investigate the acoustic wave propagation in other supracrystals such as binary systems composed by Co and/or Co/Ag nanocrystals differing by their sizes.

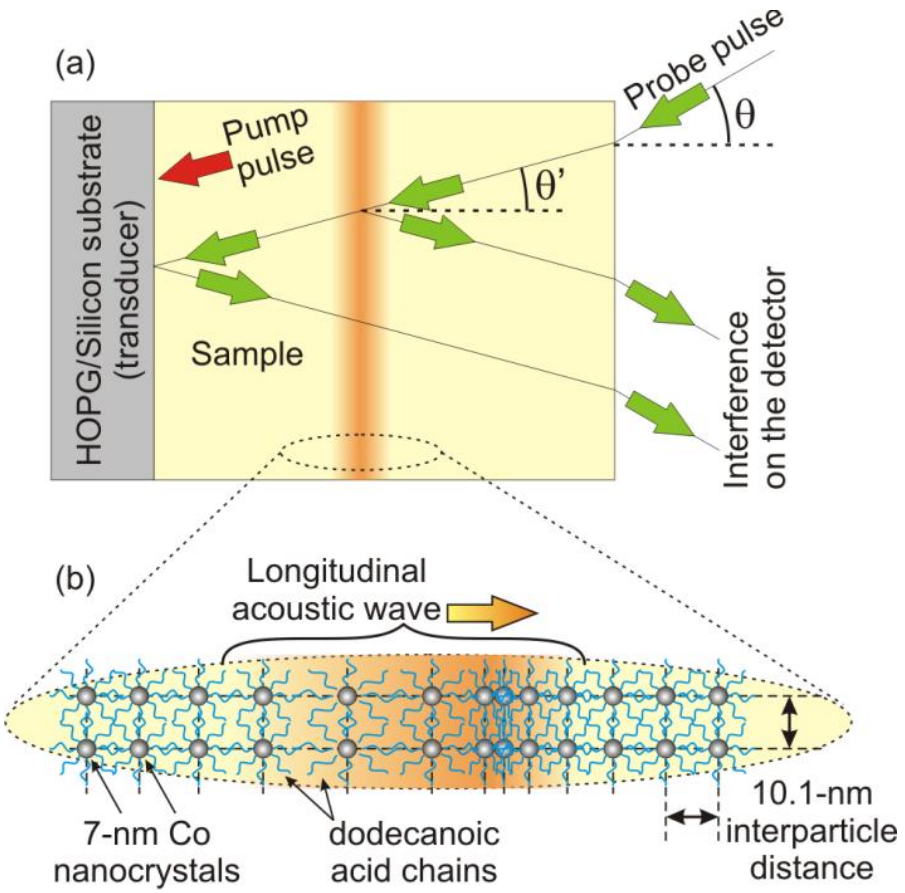

Figure 1. (a) Pictorial scheme of a picoseconds acoustics experiment. The pump beam is absorbed by the substrate (transducer), thus launching a propagating strain wave (longitudinal phonon wavepacket) which travels with the speed of sound. The incident probe beam, after refraction at the sample surface (external angle ϑ, internal angle ϑ'), is partially reflected by the substrate and by the strain wave. The detector monitors the oscillating pattern created by the interference of these two beams. (b) Close up of the supracrystal sample made of NCs, showing the compression/expansion effect characteristic of the LA waves.

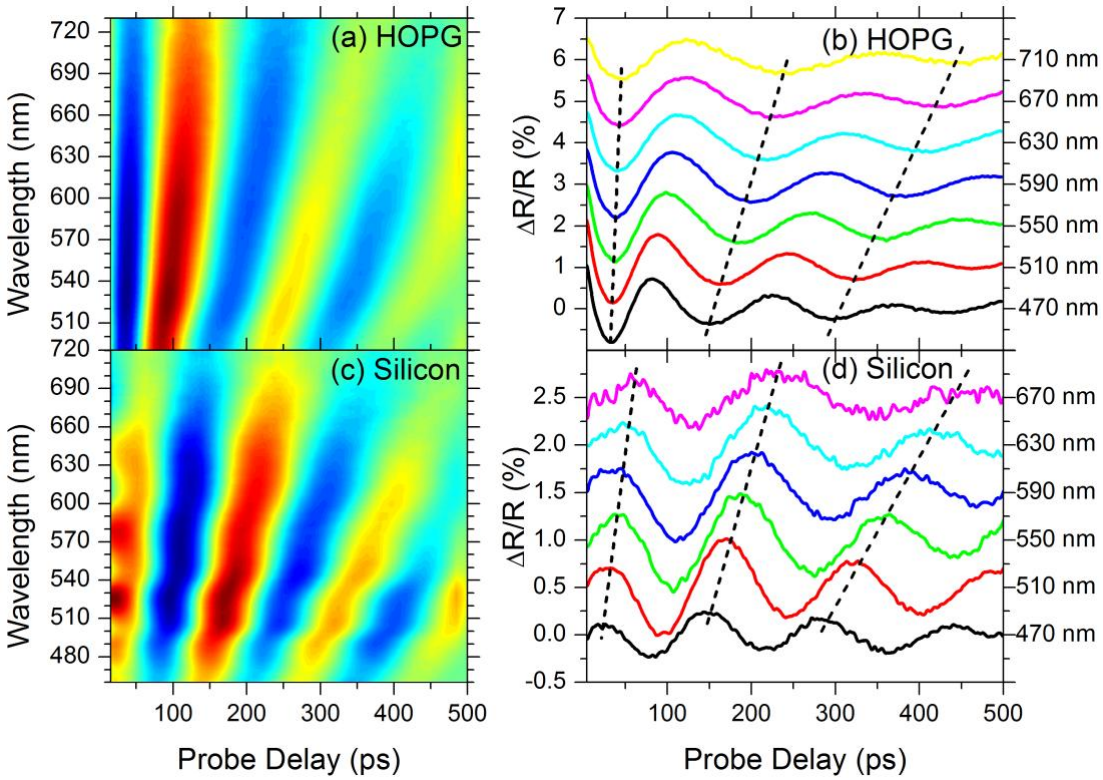

Figure 2. (a,c) 2D maps showing the $\Delta R/R$ signal as a function of both probe delay and wavelength for Co supracrystals deposited on HOPG (a) and silicon wafer (c); (b, d) corresponding $\Delta R/R$ time traces extracted from the 2D maps by horizontal cuts at various probe wavelengths. Dashed lines are a guide to the eye for highlighting the variable period of oscillation with wavelength. In all the panels only the oscillating component of the $\Delta R/R$ signal is plotted, after subtraction of the slowly varying background signal.

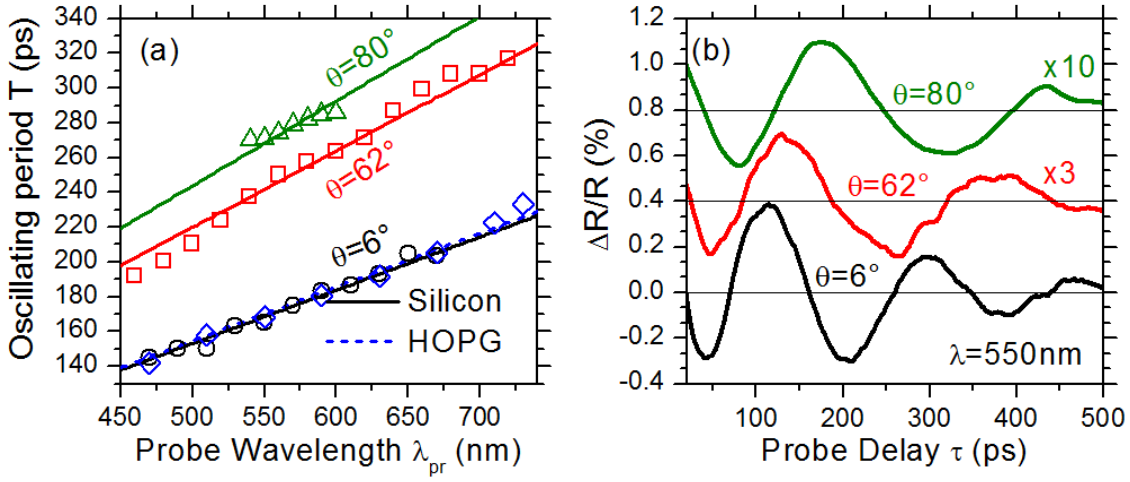

Figure 3. (a) Oscillating period T as a function of probe wavelength λ_{pr} for different angles of incidence ϑ for HOPG (blue diamonds, red squares and green triangles) and silicon (black circles) substrates. Solid and dashed lines are linear fits of the data points with zero intercept. The two datasets for ϑ=6° were extracted from Fig. 2. Visibility of the oscillating component on the $\Delta R/R$ traces is reduced for increasing incident angles, so that only the 550- to 600-nm probe wavelength region had sufficient reliability at ϑ=80° to be retained. (b) $\Delta R/R$ time traces recorded at λ_{pr} = 550 nm for the three angles of incidence on the same sample position (HOPG substrate).

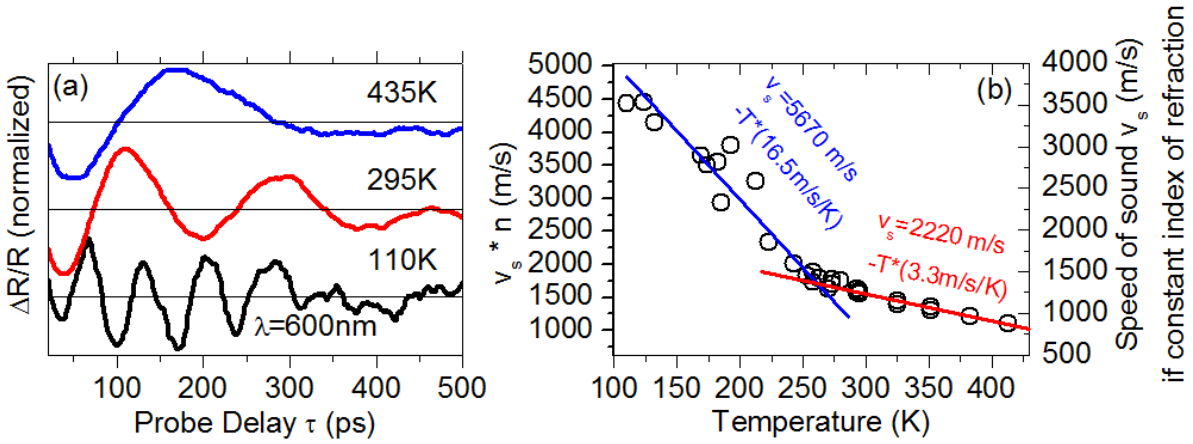

Figure 4. (a) $\Delta R/R$ dynamics as a function of sample temperature for the same probe wavelength λ_{pr}=600 nm, sample position and angle of incidence (on HOPG substrate), showing an increase in the oscillation period with temperature. (b) Product between the speed of sound and the index of refraction as a function of temperature. On the right axis the speed of sound is reported in the case no change of the index of refraction occurs with temperature.

ASSOCIATED CONTENT

Supporting Information. Materials and methods (Products, Synthesis of cobalt NCs and supracrystals, Ultrafast spectroscopy), Maxwell-Garnett mixing rule calculations. This material is available free of charge via the Internet at http://pubs.acs.org.

AUTHOR INFORMATION

Corresponding Author

* E-mail marie-paule.pileni@upmc.fr

ACKNOWLEDGMENTS

The MPP research leading to these results has received funding from Advanced Grant of the European Research Council under Grant Agreement 267129 and under the program FP-7-INFRASTRUCTURES-2008-1, "Laserlab Europe II", Contract No. 228334. GC acknowledges support from the Fondazione Cariplo ("Engineering of optical nonlinearities in plasmonic metamaterials").

REFERENCES

1. Motte, L.; Billoudet, F.; Pileni, M. P. *J Phys Chem.* **1995**, *99*, 16425-16429.

2. Murray, C. B.; Kagan, C. R.; Bawendi, M. G. *Science* **1995**, *270*, 1335-1338.

3. Whetten, R. L.; Shafigullin, M. N.; Khoury, J. T.; Schaaff, T. G.; Vezmar, I.; Alvarez, M. M.; Wilkinson, A. *Acc. Chem. Res.* **1999**, *5*, 397-406.

4. Lin, X. M.; Wang, G. M.; Sorensen, C. M. *J. Phys. Chem. B* **1999**, *103*, 5488-5492.

5. Korgel, B. A.; Fitzmaurice D. *Phys. Rev. B* **1999**, *59*, 14191-14201.

6. Pileni, M. P. *J. Phys. Chem.* **2001**, *105*, 3358-3372.

7. Courty, A.; Fermon, C.; Pileni, M. P. *Adv. Mater.* **2001**, *13*, 254-258.

8. Lisiecki, I.; Albouy, P. A.; Pileni, M. P. *Adv. Mater.* **2003**, *15*, 712-716.

9. Stoeva, S. I.; Prasad, B. L. V.; Uma, S.; Stoimenov, P .K.; Zaikovski, V.; Sorensen, C. M.; Klabunde, K. J. *J. Phys. Chem. B* **2003**, *107*, 7441-7448.

10. Compton, O. C.; Osterloh F. E. *J. Am. Chem. Soc.* **2007**, *129*, 7793-7798.

11. Park, S. Y.; Lytton-Jean, A. K. R.; Lee, B.; Weigand, S.; Schatz, G. C.; Mirkin, C. A. *Nature* **2008**, *45*, 553-556.

12. Yan, H.; Cingarapu, S.; Klabunde, K. J.; Chakrabarti, A.; Sorensen C. M. *Phys. Rev. B* **2009**, *102*, 095501-4.

13. Rupich, S. M.; Shevchenko, E. V.; Bodnarchuk, M. I.; Lee, B.; Talapin, D. V. *J. Am. Chem. Soc.* **2010**, *132*, 289-296.

14. Bian, K.; Choi, J. J.; Kaushik, A.; Clancy, P.; Smilgies, D. M.; Hanrath, T. *ACS Nano* **2011**, *5*, 2815-2823.

15. Goodfellow, B. W.; Korgel, B. A. *ACS Nano* **2011**, *5*, 2419–2424.

16. Kotov, N. A.; Meldrum, F. C.; Wu, C.; Fendler, J. H. *J. Phys. Chem.* **1994**, *98*, 2735-2738.

17. Taleb, A.; Petit, C.; Pileni, M. P. *J. Phys. Chem.* **1998**, *102*, 2214-2220.

18. Courty, A.; Mermet, A.; Albouy, P. A.; Duval, E.; Pileni, M. P. *Nat. Mater.* **2005**, *4*, 395-398.

19. Zaitseva, N.; Rong D. Z.; Leon, F. R.; Krol, D. *J. Am. Chem. Soc.* **2005**, *127*, 10221-10226.

20. Huang, W. Y.; Qian, W.; El-Sayed, M. A.; Ding, Y.; Wang, Z. L. *J. Phys. Chem. C* **2007**, *111*, 10751-10757.

21. Pileni, M. P. *Acc. of Chem. Res.* **2007**, *40*, 685-693.

22. Courty, A.; Henry, A. I.; Goubet, N.; Pileni, M. P. *Nat. Mater.* **2007**, *6*, 900-907.

23. Pileni, M. P. *Acc. Chem. Res.* 2**008**, *41*, 1799-1809.

24. Tao, A. R.; Ceperley, D. P.; Sinsermsuksakul, P.; Neureuther, A. R.; Yang, P. *Nano Lett.* **2008**, *8*, 4033-4038.

25. Lisiecki, I.; Turner, S.; Balls, S.; Pileni M. P.; Van Tendeloo G. *Chem. Mater.* **2009**, *21*, 2335-2338.

26. Podsiadlo, P.; Krylova, G.; Lee, B.; Critchley, K.; Gosztola, D. J.; Talapin, D. V.; Ashby, P. D.; Shevchenko E. V. *J. Am. Chem. Soc.* **2010**, *132*, 8953-8960.

27. Yin, K. J.; Retsch, M.; Thomas, E. L.; Boyce, M. C. *Langmuir* **2012**, *28*, 5580-5588.

28. Motte, L.; Billoudet, F.; Lacaze, E.; Pileni, M. P. *Adv. Mater.* **1996**, *8*, 1018-1020.

29. Lisiecki, I.; Pileni, M. P. *Langmuir* **2003**, *19*, 9486-9489.

30. Lisiecki, I.; Albouy, P. A.; Pileni, M. P. *J. Phys. Chem. B* **2004**, *108*, 20050-20055.

31. Thomsen, C; Strait, J.; Vardeny, Z.; Maris, H. J.; Tauc, J.; Hauser, J. J. *Phys. Rev. Lett.* **1984**, *53*, 989-992.

32. Gusev, V.; Lomonosov, A. M.; Ruello, P.; Ayouch, A.; Vaudel, G. *J. Appl. Phys.* **2011**, *110*, 124908.

33. Polli, D.; Lüer, L.; Cerullo, G. *Rev. Sci. Instrum.* **2007**, *78*, 103108.

34. Ayouch, A.; Dieudonné, X.; Vaudel, G.; Plombini, H.; Vallé, K.; Gusev, V.; Belleville P.; Ruello *ACS. Nano* **2012**, *6*, 10614-10621.

35. Ferrante, C.; Pontecorvo, E.; Cerullo, G.; Chiasera, A.; Ruocco, G.; Schirmacher W.; Scopigno, T. *Nat. Commun.* **2013**, *4*, 1793.

36. Garnett, J. C. *Philos. Trans. Roy. Soc. London* **1904**, *203*, 385-420.

37. Durvasula, L. N.; Gammon, R. W. *J. Appl.Phys.***1979,** *50*, 4339-4344.

38. Lee, K. W.; Lee, C. E.; Choi, J. Y.; Kim *J. Current Appl. Phys.* **2007**, *7*, 31-33.

39. Luedtke, W. D.; Landman, U. *J. Phys. Chem. B* **1998**, *102*, 6566-6572.

40. Mukhopadhyay, R.; Mitra, S.; Johnson, M.; Rajeev Kumar, V. R.; Pradeep, T. *Phys. Rev. B* **2007**, *75*, 075414.

SYNOPSIS

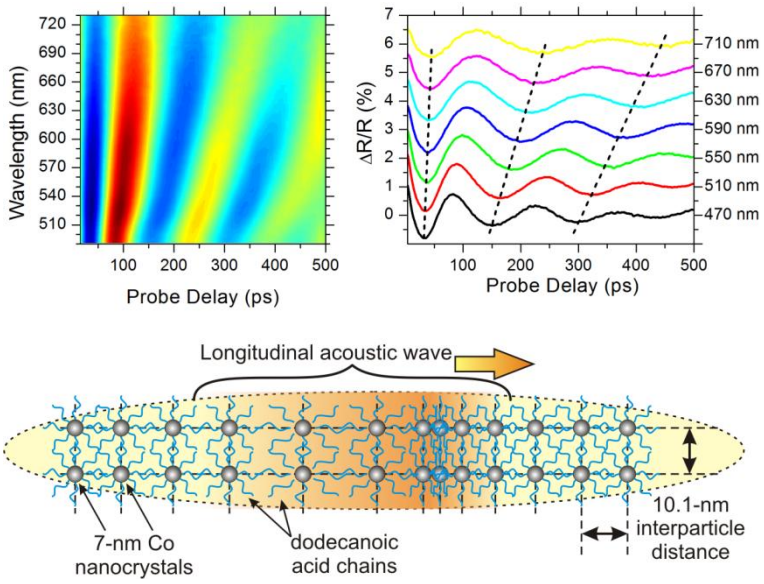
Wavelength (nm)
720
690
660
630
600
570
540
510
100
200
300
400
500
Probe Delay (ps)
ΔR/R (%)
7
6
5
4
3
2
1
0
710 nm
670 nm
630 nm
590 nm
550 nm
510 nm
470 nm
Probe Delay (ps)
Longitudinal acoustic wave
7-nm Co
nanocrystals
dodecanoic
acid chains
10.1-nm
interparticle
distance